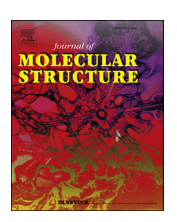
FISEVIER

Contents lists available at ScienceDirect

# Journal of Molecular Structure

journal homepage: http://www.elsevier.com/locate/molstruc



# Synthesis, structures, thermal and magnetic properties of two bis(oxalato)cuprate(II) hybrid salts containing pyridinium derivative cations



Cyrielle L.F. Dazem <sup>a</sup>, Bridget N. Ndosiri <sup>a</sup>, Emmanuel N. Nfor <sup>b</sup>, Roberto Köferstein <sup>c</sup>, Pritam Shankhari <sup>d</sup>, Boniface P.T. Fokwa <sup>d, \*\*</sup>, Justin Nenwa <sup>a, \*</sup>

- <sup>a</sup> Inorganic Chemistry Department, University of Yaounde 1, P.O. Box 812, Yaounde, Cameroon
- <sup>b</sup> Chemistry Department, University of Buea, P.O. Box 63, Buea, Cameroon
- <sup>c</sup> Institute of Chemistry, Martin Luther University Halle-Wittenberg, Kurt-Mothes-Strasse 2, 06120, Halle, Germany
- <sup>d</sup> Chemistry Department, University of California Riverside, 501 Big Springs Rd, Riverside, CA, 92521, USA

#### ARTICLE INFO

# Article history: Received 11 August 2019 Received in revised form 8 November 2019 Accepted 9 November 2019 Available online 12 November 2019

Keywords: Hybrid salts Bis(oxalato)cuprate(II) complexes Copper(II) chains Magnetic properties

#### ABSTRACT

Two bis(oxalato)cuprate(II) hybrid salts,  $(C_5H_7N_2)_2[Cu(C_2O_4)_2] \cdot 2H_2O$  (1) and  $(C_7H_{11}N_2)_2[Cu(C_2O_4)_2] \cdot 5H_2O$  (2)  $(C_5H_7N_2 = 3$ -aminopyridinium;  $C_7H_{11}N_2 = 2$ -amino-4,6-dimethylpyridinium) have been synthesized and characterized by elemental and TGA-DSC analyses, IR and UV—Vis, single-crystal X-ray diffraction and magnetic susceptibility measurements. The polymeric anionic motifs in the two salts are significantly different. In 1, stacking of  $[Cu(C_2O_4)_2]^{2^-}$  units through axial  $Cu\cdots O$  contacts (2.890 Å) yields straight Cu(II) chains, with a prolate CuO6 octahedron around Cu(II) ions, formed by two cis-chelated oxalate anions and two axial O-atoms of neighboring  $[Cu(C_2O_4)_2]^{2^-}$  units. By contrast, in 2, stacking of  $[Cu(C_2O_4)_2]^{2^-}$  units occurs via bis-bidentate oxalate groups, yielding zigzag Cu(II) chains with a distorted CuO6 coordination sphere. Thermal studies confirmed the presence of solvent water molecules in both salts. Magnetic studies revealed weak antiferromagnetic and weak ferromagnetic interactions between Cu(II) ions in 1 and 2, respectively.

© 2019 Elsevier B.V. All rights reserved.

## 1. Introduction

Organic—inorganic hybrid salts represent undeniably an important class of advanced materials that have attracted wide-spread attention within the field of crystal engineering [1–3]. They are composed of cationic organic and anionic inorganic building units. As a result of structural integration of organic cations and inorganic counterparts, these materials find wide applications in molecular electronic and spintronic [4], peculiar magnetic [5,6], optical [7,8], metallic conductivity [9] and catalytic properties [10]. Moreover, these materials may be used as model compounds for ferroelectric and ferroelastic applications [11,12]. In such salts, self-assembly processes are governed not only by intrinsic features of each ionic component, but also by non-covalent interactions including hydrogen bonds, ionic interactions,  $\pi$ - $\pi$  and/or van der

E-mail addresses: bfokwa@ucr.edu (B.P.T. Fokwa), jnenwa@yahoo.fr (J. Nenwa).

Waals interactions [13,14].

Hybrid salts involving bis(oxalato)cuprate(II) complex anions,  $[Cu(C_2O_4)_2]^{2-}$ , and organic entities as counter cations have attracted great interest in recent years due to their rich physical properties as well as their fascinating structural architectures and topologies [15–18].

Although several salts of general formula  $A_2[Cu^{II}(C_2O_4)_2] \cdot xH_2O$  (A<sup>+</sup> = aromatic iminium cation,  $0 \le x \le 5$ ) have been explored to date, the predictability and consistent formation of their networks is still in its infancy, given that bis(oxalato)cuprate(II) entities are versatile building blocks [19,20]. In most cases, the network topologies are influenced by the organic counter-cations, metal coordination spheres, pH values, guest molecules and crystallization solvents [19–21]. This flexibility of the structural topology in (organic cation)-oxalatocuprate(II) compounds bears testimony to the renewed interest in their coordination chemistry studies.

In line with our ongoing research program, we recently reported two copper(II) hybrid salts, *viz.* bis(guanidinium) bis(oxalato) cuprate(II),  $(CN_3H_6)_2[Cu(C_2O_4)_2]$  and bis(2-aminopyridinium) bis(oxalato)cuprate(II) trihydrate,  $(C_5H_7N_2)_2[Cu(C_2O_4)_2] \cdot 3H_2O$  with

<sup>\*</sup> Corresponding author.

<sup>\*\*</sup> Corresponding author.

straight and zigzag chain alignments of Cu(II) centers [22]. As a result of these findings that further confirms the structural flexibility of  $[Cu(C_2O_4)_2]^{2^-}$  anions, we have investigated other members of this family of hybrid salts with the view of not only producing new materials, but also to unravel the subtle structural and magnetic features that characterize these solids. In the present work, we report on two novel bis(oxalato)cuprate(II) hybrid salts, namely  $(C_5H_7N_2)_2[Cu(C_2O_4)_2]\cdot 2H_2O$  (1) and  $(C_7H_{11}N_2)_2[Cu(C_2O_4)_2]\cdot 5H_2O$  (2)  $(C_5H_7N_2=3$ -aminopyridinium and  $C_7H_{11}N_2=2$ -amino-4,6-dimethylpyridinium) in which the oxalate ligand exhibits different coordination modes, leading to weak antiferromagnetic and weak ferromagnetic interactions in 1 and 2, respectively.

# 2. Experimental

#### 2.1. Materials and methods

All the chemicals were purchased from commercial sources and used without further purification. The precursor  $(NH_4)_2[Cu(C_2O_4)_2]\cdot 2H_2O$  was prepared as described in the literature [23]. X-ray powder diffraction for bulk samples was carried out using a Stadi MP X-ray powder diffractometer. The parallel beam mode was used to collect the data ( $\lambda = 1.54184 \text{ Å}$ ). Elemental analyses (C, H and N) were performed using a Perkin-Elmer 240C analyzer. IR spectra (4000–400 cm<sup>-1</sup>) were recorded using an Alpha-P Bruker FT-IR spectrometer with KBr used as medium. UV/ Vis spectra were performed with a PerkinElmer Lambda 900 spectrophotometer, in water, in the range 350-900 nm  $(c = 5.57.10^{-5} \text{ mol/L})$ . Thermogravimetric analysis (TGA) and differential scanning calorimetry (DSC) were carried out on a LINSEIS STA PT-1000 thermal analyzer. The powdered sample (20 mg) was heated from 25 to 700 °C with a rate of 10 °C/min in flowing air. A Quantum Design PPMS-5XL SQUID magnetometer was used to collect magnetic susceptibility data of 1 and 2. The measurements were done at 0.3 T down to 3 K on polycrystalline samples. Diamagnetic corrections were made with Pascal's constants for all the constituent atoms as well as the contributions of samples holder [24].

# 2.2. Syntheses of 1 and 2

# 2.2.1. Synthesis of 1

A freshly prepared salt  $(NH_4)_2[Cu(C_2O_4)_2]\cdot 2H_2O$  (311 mg, 1 mmol) was added in small portions successively to a stirred aqueous solution (50 mL) of oxalic acid  $H_2C_2O_4\cdot 2H_2O$  (126 mg, 1 mmol) and 3-aminopyridine (188 mg, 2 mmol). The mixture was stirred for 1 h at room temperature before filtration. Green prismatic single crystals suitable for X-ray diffraction were isolated from the filtrate after three weeks. Yield: 405 mg (0.87 mmol, 87%) based on  $(NH_4)_2[Cu(C_2O_4)_2]\cdot 2H_2O$ . Anal. calcd (%) for 1: C, 36.09; H, 3.89; N, 12.03. Found (%): C, 36.00; H, 3.93; N, 12.09. IR data (cm $^{-1}$ ): 3460 (m), 3215 (m), 1709 (s), 1669 (s), 1637 (s), 1397 (s), 1266 (s), 789 (s), 533 (m), 484 (m). UV—Vis (H<sub>2</sub>O solution, nm): 712.

# 2.2.2. Synthesis of **2**

The copper(II) salt **2** was prepared following the above procedure by using 2-amino-4,6-dimethylpyridine (244 mg, 2 mmol) instead of 3-aminopyridine. Green-needle single crystals suitable for X-ray diffraction were collected after three weeks. Yield: 490 mg (0.85 mmol, 85%) based on (NH<sub>4</sub>)<sub>2</sub>[Cu(C<sub>2</sub>O<sub>4</sub>)<sub>2</sub>]·2H<sub>2</sub>O. Anal. calcd (%) for **2**: C, 37.53; H, 5.60; N, 9.73. Found (%): C, 37.82; H, 5.63; N, 10.06. IR data (cm<sup>-1</sup>): 3318 (m), 3157 (m), 1666 (m), 1601 (s), 1419 (m), 1279 (m), 790 (m), 491 (m). UV—Vis (H<sub>2</sub>O solution, nm): 707.

#### 2.3. Crystal structure determination

Single-crystal X-ray diffraction intensity data for 1 and 2 were collected on a Bruker APEX II CCD diffractometer using graphitemonochromatized Mo-K $\alpha$  radiation ( $\lambda = 0.71073$  E) at 100(2) K. The X-ray intensities were corrected for absorption using a semiempirical procedure [25]. Both structures were solved by direct methods and refined on  $F^2$  by full-matrix least-square techniques using SHELX-2014 program package [26]. All non-hydrogen atoms were refined anisotropically. The positions of hydrogen atoms were added in idealized geometrical positions for the organic cations except for 2 CH<sub>3</sub> groups (C26 and C27) in 2 which were located from the difference Fourier map to assign appropriate orientation. The positions of hydrogen atoms from the water molecules were assigned from the electronic density map generated by Fourier difference and they were refined freely. In 2, some water molecules show disorder (not accounted for in our refinement) leading to the slightly high peaks (ca. 1.5 e/Å<sup>3</sup>) in the difference Fourier map. The DIAMOND program [27] was used to deal with the processed crystallographic data and artwork representations. Details of the crystallographic data and structure refinement parameters for 1 and 2 are summarized in Table 1 and selected bond lengths and angles in Table 2.

#### 3. Results and discussion

#### 3.1. Formulation of 1 and 2

Reaction of oxalic acid. 3-aminopyridine and  $(NH_4)_2[Cu(C_2O_4)_2]$ .  $2H_2O$  in water at room temperature yielded  $(C_5H_7N_2)_2[Cu(C_2O_4)_2]$ . 2H<sub>2</sub>O (1) which was isolated as green prismatic crystals. Under the same experimental conditions and using 2-amino-4,6dimethylpyridine in lieu of 3-aminopyridine,  $(C_7H_{11}N_2)_2[Cu(C_2O_4)_2]\cdot 5H_2O$  (2) was isolated as green needle-like crystals. Bulk samples of the described compounds were each studied by means of X-ray powder diffraction analysis (Fig. S1). The experimental powder X-ray diffraction (PXRD) patterns of polycrystalline samples of 1 and 2 reveal a slight difference with those simulated from the single-crystal X-ray diffraction data, indicating that phase impurities can be negligible in the bulk materials. In addition, the elemental analysis results were in agreement with the chemical formulations of 1 and 2, with the synthetic procedures shown in Scheme 1. Formation of these salts can be understood in terms of the combination of two chemical processes which are, protonation of the imine groups of the pyridine derivatives (DerPy) by oxalic acid, producing iminium cations (DerPy-H)<sup>+</sup> and, exchange of the ammonium cations of the precursor  $(NH_4)_2[Cu(C_2O_4)_2] \cdot 2H_2O$  with the iminium ones.

### 3.2. Structure description of 1 and 2

The hybrid salts  $(C_5H_7N_2)_2[Cu(C_2O_4)_2]\cdot 2H_2O$  (1) and  $(C_7H_{11}N_2)_2[Cu(C_2O_4)_2]\cdot 5H_2O$  (2) crystallize in the monoclinic system with space group  $P2_1/c$  and triclinic system with space group  $P1_1$ , respectively. The crystal structure details of 1 and 2 are depicted in Fig. 1, with each metal atom in a six-coordinate environment.

The crystal structure of **1** (Fig. 1a) consists of one bis(oxalato) cuprate(II) complex,  $[Cu(C_2O_4)_2]^{2-}$ , two 3-aminopyridinium cations,  $(C_5H_6N_2)^+$ , and two lattice water molecules. The Cu(II) ion is located at the inversion center and is bonded to four oxygen atoms (O11, O12, O11', O12') from two oxalate(2-) ligands (average Cu–O length: 1.932 Å) in the equatorial plane and weakly interacts with two axial O-atoms of neighboring  $[Cu(C_2O_4)_2]^{2-}$  units to build a prolate  $CuO_6$  octahedron, with regular axial  $Cu\cdots O$  contacts of

**Table 1**Crystal data and structure refinements for **1** and **2**.

Compound	1	2
Empirical formula	C <sub>14</sub> H <sub>18</sub> CuN <sub>4</sub> O <sub>10</sub>	C <sub>18</sub> H <sub>32</sub> CuN <sub>4</sub> O <sub>13</sub>
Formula weight	465.86	576.02
T(K)	100(2)	100(2)
$\lambda$ (Å)	0.71073	0.71073
Crystal system	Monoclinic	Triclinic
Space group	$P2_1/c$	P-1
Unit Cell parameters		
a (Å)	3.6658(10)	9.5727(3)
b (Å)	21.3317(7)	10.9847(4)
c (Å)	11.2592(4)	13.6468(5)
α(°)	90	108.0960(10)
$\beta$ (°)	90.165(10)	96.2090(10)
γ (°)	90	107.8150(10)
$V(Å^3)$	880.44(5)	1265.46(8)
Z	2	2
$\mu  (\mathrm{mm}^{-1})$	1.307	0.934
F(000)	478	602
Crystal size (mm)	$0.18 \times 0.30 \times 0.30$	$0.09 \times 0.10 \times 0.17$
$\theta$ range for data collection (°)	2.045-31.456	1.611-31.476
Index ranges	-5 < h < 5, -24 < k < 30, -15 < l < 16	-9 < h < 14, -15 < k < 15, -20 < l < 19
Total reflections	2900	8184
Unique reflections ( $R_{int}$ )	2691(0.0171)	7311(0.0190)
Refinement method	full-matrix least squares on F <sup>2</sup>	full-matrix least squares on F <sup>2</sup>
Data/restraints/parameters	2900/0/133	8184/21/390
Goodness-of-fit (GOF) on F <sup>2</sup>	1.114	1.106
R factor $[I > 2\sigma(I)]$	$R_1 = 0.0284$ , $wR_2 = 0.0671$	$R_1 = 0.0406$ , w $R_2 = 0.1233$
R factor (all data)	$R_1 = 0.0311$ , w $R_2 = 0.0680$	$R_1 = 0.0446$ , w $R_2 = 0.1261$
Max and min residual electron density (e/Å <sup>3</sup> )	0.605 and -0.323	1.512 and -0.957

 Table 2

 Selected bond lengths (Å) and angles ( $^{\circ}$ ) within the coordination spheres around the metal centers in 1 and 2.

Compound 1			
Cu1-O11	1.9251(9)	O11-Cu1-O11_01 <sup>i</sup>	180.00(1)
Cu1-O11_01 <sup>i</sup>	1.9251(9)	O11-Cu1-O12_01 <sup>i</sup>	94.21(4)
Cu1-O12	1.9379(9)	012-Cu1-012_01 <sup>i</sup>	180.00(1)
Cu1-012_01 <sup>i</sup>	1.9379(9)	012-Cu1-011_01 <sup>i</sup>	94.21(4)
C11-C12	1.5525(18)	O11-Cu1-O12	85.79(4)
Cu···O12	2.8900(1)	O11_01 <sup>i</sup> —Cu1—O12_01 <sup>i</sup>	85.79(4)
C11_01 <sup>i</sup> -C12_01 <sup>i</sup>	1.5525(18)		
Compound 2			
Cu1-011	1.9804(11)	016-Cu1-015	76.74(4)
Cu1-O14	1.9540(11)	018-Cu1-017	77.87(5)
Cu1-015	2.3292(12)	014-Cu1-011	82.94(5)
Cu1-O16_01i	2.0043(12)	011-Cu1-016	173.85(5)
Cu1-017	2.3183(13)	015-Cu1-017	157.94(4)
Cu1-O18	1.9726(12)	014-Cu1-018	170.38(5)
C13-C14	1.5544(19)		
C11-C11_01 <sup>i</sup>	1.5610(3)		
C12-C12_01 <sup>i</sup>	1.5650(4)		

 $Symmetry\ transformations\ used\ to\ generate\ equivalent\ atoms;\ (i)\ -x,\ 1-\ y,\ 1-\ z\ for\ \textbf{1}\ and\ (i)\ 1-x,\ 1-y,\ -z\ for\ \textbf{2}.$ 

1<sup>st</sup> step: Protonation of imine group of the pyridine derivatives

$$2 \text{ DerPy} + \text{H}_2\text{C}_2\text{O}_4 \xrightarrow{\text{H}_2\text{O}} \text{(DerPy-H)}_2\text{C}_2\text{O}_4$$

2<sup>nd</sup> step: Exchange of NH<sub>4</sub><sup>+</sup> with DerPy-H<sup>+</sup>

$$(DerPy-H)_2C_2O_4 + (NH_4)_2[Cu(C_2O_4)_2] \cdot 2H_2O \xrightarrow{H_2O}$$
 
$$(DerPy-H)_2[Cu(C_2O_4)_2] \cdot nH_2O + (NH_4)_2C_2O_4$$

**Scheme 1.** Two-step synthesis of salts 1 and 2.

2.890 Å. The basal  $CuO_4$  plane is planar due to symmetry restriction, and the O-Cu-O bite angle within the plane is  $85.790(1)^\circ$ , a value

which is similar to those found in previously reported compounds [20,28,29].

The asymmetric unit of **2** (Fig. 1b) consists of a central copper(II) ion, two halves of bis-bidentate oxalate anion, one bidentate oxalate anion, two 2-amino-4,6-dimethylpyridinium cations and five lattice water molecules. The Cu(II) center experiences a pseudo-octahedral coordination geometry by three chelating oxalate(2-) ions with the well-established helical orientation within the complex anion. As in **1**, each Cu(II) ion has four nearest neighbors at short distances Cu1-O11, Cu1-O14, Cu1-O16 and Cu1-O18 ( $\leq$ 2 Å), defining the highest singly occupied molecular orbital (SOMO), and two other oxygen atoms (O15, O17) at longer distances (2.3 Å) but much shorter than in **1**. The coordination sphere in **2** can be described as a distorted CuO<sub>6</sub> octahedron. Moreover, with the value obtained for the O15-Cu1-O17 bond angle (157°) being quite distant from 180°, the CuO6 octahedron in **2** is not only axially

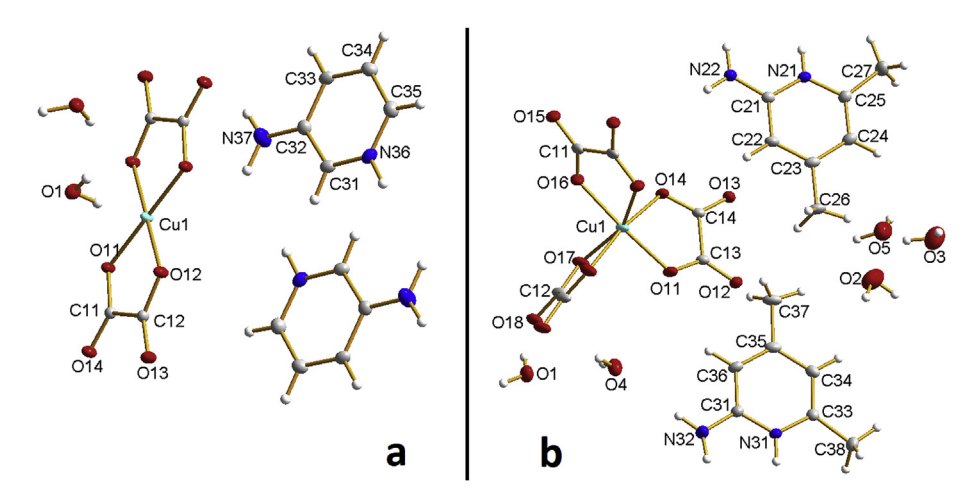


Fig. 1. Constitutive entities of 1 (a) and 2 (b) with the atom numbering scheme. Displacement ellipsoids are drawn at the 50% probability level.

elongated, it is also axially bent [30]. In 2, there are two kinds of oxalates: two bridging (the ones with C11-C11 and C12-C12 bonds) and one pendant (with C13-C14 bond). The bonding of Cu(II) ion to the pendant oxalate is realized through two short Cu-O bonds (Cu-O11, Cu-O14), whereas the bonding of the Cu(II) ion to the bridging oxalates is built from a short and a long Cu-O bonds. The long bonds Cu-O17 (in oxalate with C12) and Cu-O15 (in oxalate with C11) are related by an inversion center at the half of the C-C bond of the bridging oxalates. The structure of 2 has a noteworthy aspect: to the best of our knowledge, no example of pyridinium salts in which the copper(II) ion is surrounded by three coordinated oxalate(2-) groups has been reported hitherto. Of all the 73 hits found in CSD in which the coordination sphere of Cu sites is comparable to the present case, the organic cations compensating the charge of the anionic building block were rather ammonium cations [31,32].

The supramolecular anionic entities in **1** and **2** are illustrated in Fig. 2. In **1**,  $[Cu(C_2O_4)_2]^{2^-}$  entities are polymerized through crystallographic symmetry-related O12 atoms, forming straight Cu(II) chains with regular spacing of  $Cu\cdots Cu = 3.666(1)$  Å, in accordance with the  $Cu\cdots Cu$  distances [3.697(7) and 3.582(5) Å] for analogous salts [20,22]. By contrast, in **2**, adjacent  $[Cu(C_2O_4)_2]^{2^-}$  entities are bridged by oxalate anions in a bis-bidentate mode to form zigzag chain alignments of Cu(II) centers in which the  $[Cu(C_2O_4)_3]$  units are alternatively lambda and delta symmetry, ending up in a non-

chiral structure, the average Cu···Cu distance being 5.585 Å.

The crystal structures of **1** and **2** are stabilized by multiple intermolecular hydrogen bonds (Fig. 3) between crystallization water molecules, cations and anions with the  $O-H\cdots O$  and  $N-H\cdots O$  distances in the ranges of 2.80(1)-3.05(1) Å and 2.79(2)-2.99(2) Å, respectively. Relevant hydrogen bond lengths and angles for **1** and **2** are presented in Table 3.

# 3.3. IR and UV-Vis spectra of 1 and 2

# 3.3.1. IR spectra

The IR spectrum of **1** exhibits two broad and weak absorption bands at 3551 and 3460 cm<sup>-1</sup> corresponding to  $\nu_{(N-H)}$  of the 3-aminopyridinium ion, at 3319 and 3215 cm<sup>-1</sup> corresponding to  $\nu_{(O-H)}$  of the water molecules. Complex **2** shows broad and weak absorption bands at 3318 and 3157 cm<sup>-1</sup> attributable to  $\nu_{(N-H)}$  of the 2-amino-4,6-dimethylpyridinum ion and to  $\nu_{(O-H)}$  of the water molecules respectively [33]. In this last complex, a strong and sharp band at 1600 cm<sup>-1</sup> corresponds to  $\delta_{(N-H)}$  vibration [34]. No strong and sharp absorption band around 1611 cm<sup>-1</sup> assigned to the C=N vibrations of pyridine ring of 3-aminopyridinium and 2-amino-4,6-dimethylpyridinium cations was observed, thus suggesting that the pyridine group has been protonated [35].

The strong absorption bands at 1709, 1669, 1637 cm<sup>-1</sup> for **1** and the one at 1666 cm<sup>-1</sup> for **2** can be attributed to the  $v_{asym(COO)}$ 

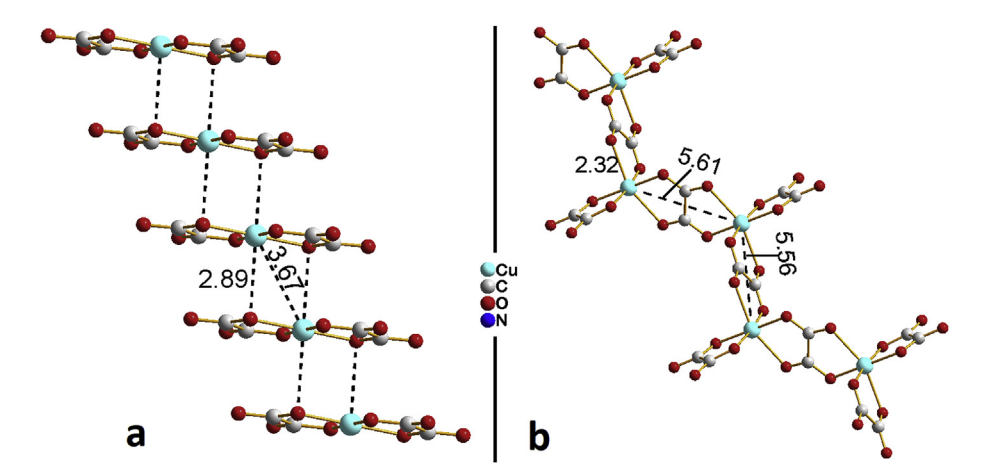


Fig. 2. Straight (a) and zigzag (b) chains of Cu(II) centers in 1 and 2, respectively.

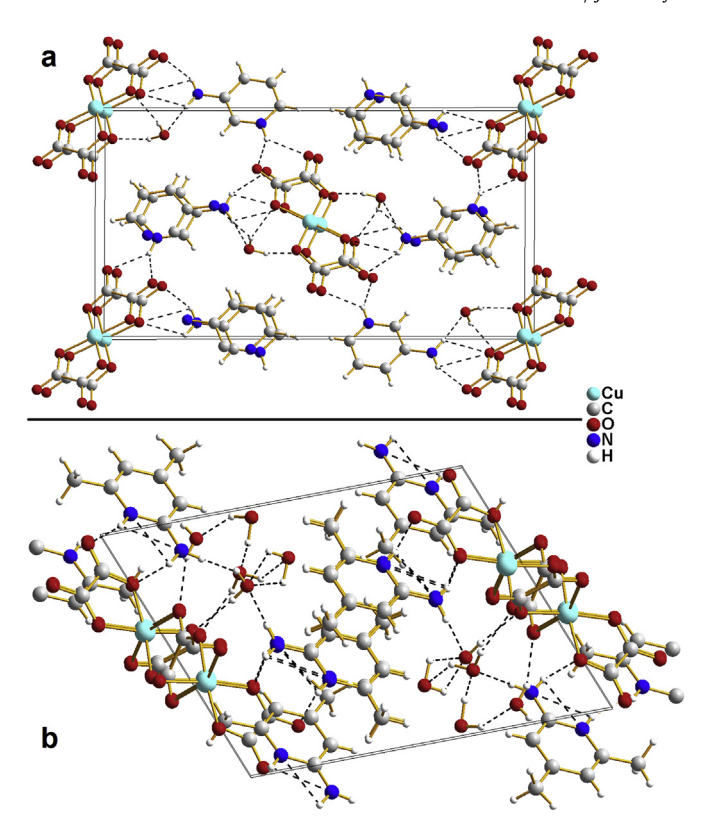


Fig. 3. Packing diagrams of 1 (a) and 2 (b) showing  $O-H\cdots O$  and  $N-H\cdots O$  hydrogen bonds (dashed lines).

Table 3
Hydrogen bond lengths (Å) and angles (°) for 1 and 2

Trydrogen bond rengths (A) and angles (7) for T and Z.						
D-H-A	d(D-H)	d(H-A)	d(D-A)	<(DHA)		
$(C_5H_7N_2)_2[Cu(C_2O_4)_2]\cdot 2H_2O(1)$						
N36-H36-O13	0.94	2.25	2.924(16)	129		
N36-H36-014	0.94	1.96	2.801(15)	149		
N37-H37A-01	0.94	2.03	2.966(18)	175		
N37-H37B-O14	0.85	2.27	3.047(17)	153		
O1-H1A-O12	0.89	2.02	2.885(14)	165		
O1-H1B-O11	0.82	2.24	2.984(15)	152		
$(C_7H_{11}N_2)_2[CuC_2O_4)_2] \cdot 5H_2O(2)$						
N21-H26-O12i	0.88(1)	1.93(2)	2.794(18)	169		
N22-H29B-O4	0.90(1)	2.13(1)	2.998(2)	167		
N22-H29A-011 <sup>i</sup>	0.90(2)	2.04(2)	2.911(19)	164		
01-H1A-012	0.79(2)	2.06(2)	2.846(18)	173		
O3-H3A-O2	0.85(2)	2.28(2)	2.862(3)	126		
O4-H4B-O16	0.79(2)	2.00(2)	2.792(2)	175		

Symmetry transformations used to generate equivalent atoms (D, donor; A, acceptor): (i) = 1 + x, y, z for **2**.

stretching vibrations [34,36]. The bands at 1396 cm $^{-1}$  observed for 1 and at 1419 cm $^{-1}$  observed for 2 are due to  $v_{\text{sym}(C-O)} + \nu_{(C-C)}$  stretching vibrations. The bands appearing at 1265 and 789 cm $^{-1}$  in 1, and at 1279 and 791 cm $^{-1}$  in 2 can be assigned to  $v_{\text{sym}(C-O)} + \delta_{(COO)}$  vibrations [34,36]. The strong bands at 533 cm $^{-1}$  and 485 cm $^{-1}$  in 1 and at 491 cm $^{-1}$  in 2 can be assigned to  $\nu_{(Cu-O)}$  vibration [36].

# 3.3.2. UV-vis spectra

The visible spectra of Cu(II) complexes **1** and **2** were recorded in distilled water. Each of these complexes revealed a broad peak around 712 nm (14044 cm $^{-1}$ ) for **1** and 707 nm (14144 cm $^{-1}$ ) for **2**. These bands can be assigned to  $^2E_g \rightarrow ^2T_{2g}$  transition [37], which is consistent with an octahedral geometry around the central Cu $^{2+}$ 

ion in both hybrid salts [38]. This assignment is in agreement with the X-ray structural results.

## 3.4. Thermal analyses of 1 and 2

Results of the thermal analyses (TGA and DSC) of powder samples 1 and 2 are depicted in Fig. 4. Both compounds show two main decomposition steps. The first step is associated with endothermic effect and the second one with exothermic effect. For 1, the TGA curve (Fig. 4 a) shows a first mass loss of 3.8% (calcd. 3.9%) in the range 50-100 °C, due to the release of one lattice water molecule. Above 230 °C, the second mass loss of 35.8% (calcd. 36.1%) occurs, which corresponds to the decomposition of the framework and formation of a residue. For 2, the TGA curve (Fig. 4) b) shows a first mass loss of 9.1% (calc. 9.4%) between 50 and 100 °C, corresponding to the release of three lattice water molecules. As in 1, above 230 °C, a second mass loss of 41.9% (calcd. 42.1%) takes place and the decomposition of the framework is completed, leading to another residue. The measured PXRD patterns of both residues appeared to be very similar to the reported PXRD pattern of CuO (Fig. S2).

# 3.5. Magnetic properties of 1 and 2

Magnetic measurements of **1** and **2** were carried out at 0.3 T from room temperature down to 3 K. As illustrated in Fig. 5, **1** and **2** have different magnetic behaviors, as can be expected if structure-

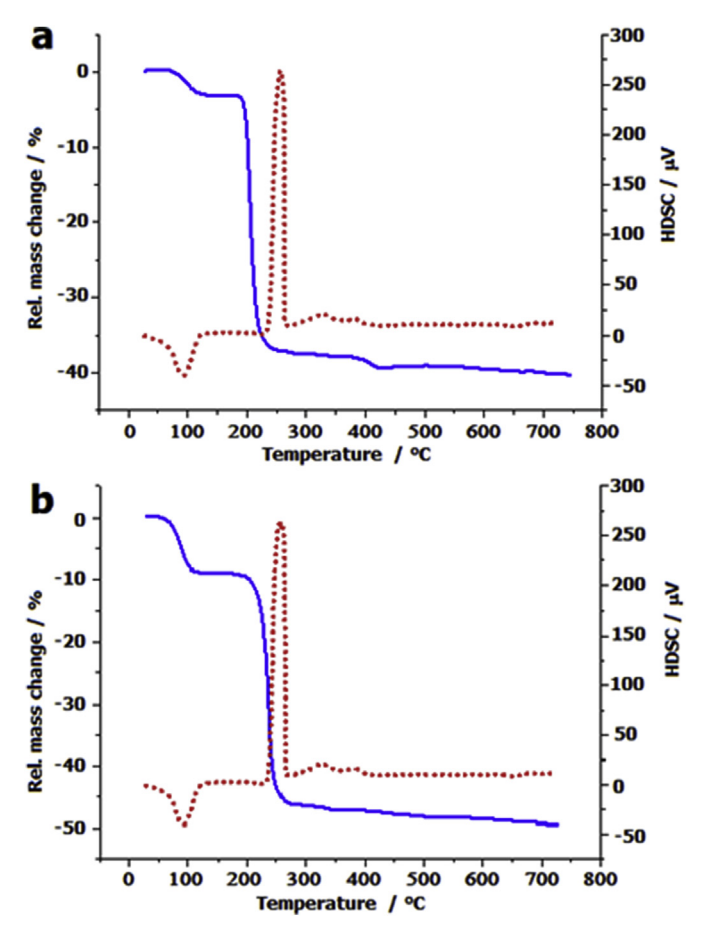


Fig. 4. TGA (blue) and DSC (red) diagrams for 1 (a) and 2 (b).

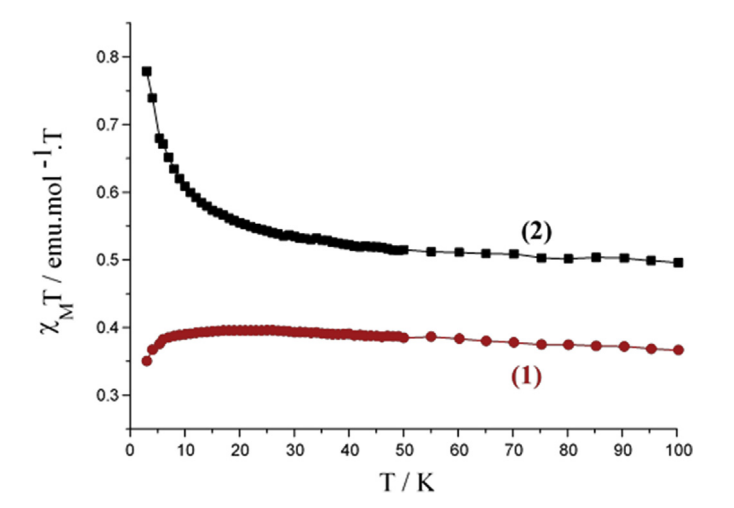


Fig. 5. Temperature-dependent magnetic behavior of 1 (red) and 2 (black).

activity relationships are considered, i.e. the different chains built by the magnetic centers will affect the magnetic properties as demonstrated for many other complexes in recent years [22,39–42]. The  $\chi_M$  T vs T plot is commonly used to probe the magnetic interactions between paramagnetic centers: If the  $\chi_M T$ values decrease with decreasing temperature, this indicates an antiferromagnetic interaction, while an increase of the  $\chi_M T$  values with a decrease in temperature leads to a ferromagnetic interaction [42]. Furthermore, Oshio and Nagashima [42] demonstrated through theoretical calculations on 1D chains of copper(II) complexes using the Heisenberg linear chain model, that the weak antiferromagnetic interaction in the chain is due to the long axial Cu-O bond length (ca. 2.54 Å), which causes a small induction of the spin on the  $d_{Z^z}$  orbital of the nearby complex. Likewise, they argued that a shorter axial Cu-O bond length (ca. 2.31 Å) would lead to stronger interactions because the orthogonality between the  $d_{Z^z}$  orbital of the spin induced on the oxalate and the  $d_{x^z-y^z}$ orbital of the primary spin is responsible for the ferromagnetic interaction. However, when the orthogonality of the two orbitals is not strictly kept this causes a weak ferromagnetic interaction.

For **1**, the room temperature  $\chi_M T$  value is 0.37 emu.mol<sup>-1</sup>.K, which perfectly matches the calculated value of one isolated Cu<sup>2+</sup> ion (0.37 emu.mol<sup>-1</sup>.K, S = 1/2), in accordance with the structural description of well separated mononuclear complexes (not a dinuclear complex) that weakly interact with each other. Upon cooling, the  $\chi_M T$  value increases very slowly up to a maximum value of 0.39 emu.mol<sup>-1</sup>.K at around 7 K and drops sharply to 0.35 emu.mol<sup>-1</sup>.K at 3 K, revealing therefore the occurrence of weak antiferromagnetic interactions between the Cu(II) ions at low temperatures, as observed in many other complexes containing straight chain alignments of Cu centers [22,42]. According to the above description for the occurrence of weak antiferromagnetic interactions in straight Cu(II) chains, a long axial Cu–O bond length is necessary, and indeed it is realized at an even longer Cu–O distance of 2.89 Å in **1** (Fig. 2a).

At room temperature, the  $\chi_M T$  value of **2** is about 0.50 emu.mol<sup>-1</sup>.K, a value which is higher than the expected 0.37 emu.mol<sup>-1</sup>.K value mentioned above, but far less than the expected value for a dinuclear complex. Upon lowering the temperature,  $\chi_M T$ gradually increases from 0.50 emu.mol<sup>-1</sup>.K at 100 K to 0.54 emu.mol<sup>-1</sup>.K at around 20 K, and then abruptly increases to reach the value 0.78 emu.mol<sup>-1</sup>.K at 3 K. This temperature-dependent behavior indicates the occurrence of weak ferromagnetic interactions between the Cu(II) ions [43]. Interestingly, the above mentioned explanation for the occurrence of weak ferromagnetism in Cu(II) chains is well verified for the structure of 2 as a much shorter axial Cu-O bond length is found (2.33 Å) that perfectly matches the distance reported by Oshio and Nagashima [42]. Moreover, it has been demonstrated for this family of complexes (with short axial Cu-O bond length) that for values of the bond angle at the axial copper to oxalate-oxygen ( $\beta$ ) greater than 109.5°, antiferromagnetic coupling is favored, whereas values smaller than 109.5° give rise to ferromagnetic interactions [32,44]. Therefore, the  $\beta$  value (108.8°) in **2** further confirms the ferromagnetism observed. The magneto-structural data of some oxalato-bridged dicopper(II) complexes [32,42,44-50] are listed in Table 4. They nicely confirm that the values of the bond angle at the axial copper to oxalate-oxygen ( $\beta$ ) and the axial copper to oxalate oxygen bond length are the main structural factors governing the nature of the magnetic coupling.

 Table 4

 Selected structural data for oxalato-bridged copper(II) complexes having the out-of-plane exchange pathway.

Compound <sup>a</sup>	Donor set <sup>b</sup>	$d_{Cu-O(ax)}^{c}(A)$	β <sup>d</sup> (°)	$d_{Cu-O}^{e}(A)$	d <sub>Cu Cu</sub> f (Å)	Magn. coupling <sup>g</sup>	Ref.
Cu <sub>2</sub> (bpca) <sub>2</sub> (ox)	N <sub>3</sub> O <sub>2</sub>	2.26	107.5	_	5.44	F	[44]
$[Cu_2(bpca)_2(H_2O)_2(ox)] \cdot 2H_2O$	$N_3O_2O'$	2.41	106.9	1.96	5.63	F	[45]
$[(CH_3)_4N]_2[Cu(ox)_2] \cdot H_2O$	$O_6$	2.38	106.9	1.97	5.59	F	[32]
[Cu2(bpcam)2(H2O)2(ox)]	$N_3O_2O'$	2.44	106.6	1.97	5.68	F	[46]
$(C_7H_{11}N_2)_2[Cu(ox)_2] \cdot 5H_2O(2)$	$O_6$	2.32	108.8	1.98	5.61	F	This work
[Cu(bipy)(ox)]·2H <sub>2</sub> O	$N_2O_4$	2.31	108.3	1.95	5.56	F	[47]
$Cu(py)_2(ox)$	$N_2O_4$	2.27	108.0	1.94	5.46	F	[42]
$Cu(2-ampy)_2(ox)$	$N_2O_4$	2.38	107.8	1.99	5.63	F	[48]
$Cu(isq)_2(ox)$	$N_2O_4$	2.23	109.5	2.003	5.48	F	[49]
$(C_5H_7N_2)_2[Cu(ox)_2] \cdot 2H_2O(1)$	$O_6$	2.89	112.2	1.93	3.67	AF	This work
$Cu(4-ampy)_2(ox)$	$N_2O_4$	2.35	109.7	2.03	5.66	AF	[48]
$Cu(3-ampy)_2(ox)$	$N_2O_4$	2.17	111.0	2.05	5.46	AF	[48]
$[Cu_2(bipy)_2(H_2O)_2(ox)](CF_3SO_3)_2$	N <sub>2</sub> O <sub>2</sub> O'O"	2.36	110.7	1.97	5.13	AF	[50]

<sup>&</sup>lt;sup>a</sup> Abbreviations of the ligands: bpca: bis(2-pyridylcarbonyl)amidate; ox: oxalate; bpcam: bis(2.pyrimidylcarbonyl)amidate; bipy: 2,2'-bipyridine; py: pyridine; 2-ampy: 2-aminopyridine; isq: isoquinoline; 4-ampy: 4-aminopyridine; 3-ampy: 3-aminopyridine.

<sup>&</sup>lt;sup>b</sup> The first four atoms form the basal/equatorial plane.

<sup>&</sup>lt;sup>c</sup> Value of the axial copper to oxalate-oxygen.

<sup>&</sup>lt;sup>d</sup> Bond angle at the axial oxalate—oxygen (Cu—O—C).

<sup>&</sup>lt;sup>e</sup> Value of the equatorial copper to oxalate-oxygen.

f Copper—copper distance across the bridging oxalato.

 $<sup>^{\</sup>rm g}$  F = ferromagnetic interactions; AF = antiferromagnetic interactions.

#### 4. Conclusion

paper, two organic-inorganic hybrid this salts  $(C_5H_7N_2)_2[Cu(C_2O_4)_2]\cdot 2H_2O$  (1) and  $(C_7H_{11}N_2)_2[Cu(C_2O_4)_2]\cdot 5H_2O$ (2)  $(C_5H_7N_2 = 3$ -aminopyridinium and  $C_7H_{11}N_2 = 2$ -amino-4,6dimethylpyridinium) have been presented together with their spectroscopic, thermal and magnetic results. In 1, the  $[Cu(C_2O_4)_2]^{2-1}$ units polymerize through long axial Cu···O contacts of 2.890 Å, thus generating a chain structure with straight alignment of Cu(II) centers. By contrast, in **2**,  $[Cu(C_2O_4)_2]^{2^-}$  entities are bridged by oxalate ligands in bis(bidentate) coordination mode, yielding zigzag copper(II) chains. The distinct polymeric anionic motifs in the two compounds have marked effects on their magnetic properties. 1 exhibits weak antiferromagnetic interactions whereas 2 exhibits weak ferromagnetic interactions.

These findings clearly suggest that the magnetic properties of oxalatocuprate(II) salts are sensitive to the type of cationic species and the coordination environment of the metal ions within the structures. It is worth noting finally, that the present report in all likelihood, lends good grounds to anticipate that a lot is still to be done and understood in this class of hybrid materials, given the wide range of cations that are susceptible to cancel the negative charge of the infinite oxalatocuprate(II) chains. Therefore, one may expect this assessment to be extendable, not only to homologous organic cations, but to small inorganic charged species such as hydronium ( $H_3O^+$ ) cations as well. Materials of this type, no doubt, could be well-adapted models in the exploration of the concept of one-dimensional proton conducting solids (1D-PCS) [51-54]. Work in this direction is in progress in our lab.

# Acknowledgements

The authors would like to thank Prof. Christian Robl (Institute of Inorganic and Analytical Chemistry, Jena University, Germany) for assistance with the magnetic measurements. This work was supported by the startup to BPTF at UC Riverside and the National Science Foundation Career Award to BPTF (no. DMR-1654780).

# Appendix A. Supplementary data

Supplementary data to this article can be found online at https://doi.org/10.1016/j.molstruc.2019.127399.

# References

- [1] X.M. Zhang, M.L. Tong, X.M. Chen, Angew. Chem. Int. Ed. 41 (2002) 1029.
- [2] I. Matulková, J. Cihelka, M. Pojarová, K. Fejfarová, M. Dušek, P. Vaněk, J. Kroupa, R. Krupková, J. Fábry, I. Němec, CrystEngComm 14 (2012) 4625.
- [3] Y. Sun, Y. Zong, H. Ma, A. Zhang, K. Liu, D. Wang, W. Wang, L. Wang, J. Solid State Chem. 237 (2016) 225.
- [4] A.H. Pedersen, M. Julve, J. Martínez-Lillo, J. Cano, E.K. Brechin, Dalton Trans. 46 (2017) 16025.
- [5] P.G. Lacroix, I. Malfant, Chem. Mater. 13 (2001) 441.
- [6] M. Clemente-Leon, E. Coronado, C. Marti-Gastaldo, F.M. Romero, Chem. Soc. Rev. 40 (2011) 473.
- [7] I. Matulková, J. Cihelka, K. Fejfarová, M. Dušek, M. Pojarová, P. Vaněk, J. Kroupa, M. Šála, R. Krupková, I. Němec, CrystEngComm 13 (2011) 4131.
- [8] M. Clemente-Leon, E. Coronado, J.R. Galan-Mascaros, E. Canadell, Inorg. Chem. 39 (2000) 5394.
- [9] E. Coronado, J.R. Galan-Mascaros, C.J. Gomez-Garcia, V. Laukhin, Nature 408

- (2000) 447.
- [10] O.M. Yaghi, M. O'Keeffe, N.W. Ockwig, H.K. Chae, M. Eddaoudi, J. Kim, Nature 423 (2003) 705.
- [11] W. Rekik, H. Naıli, T. Mhiri, T. Bataille, Mater. Res. Bull. 43 (2008) 2709.
- [12] E. Pardo, C. Train, H. Liu, L.M. Chamoreau, B. Dkhil, K. Boubekeur, F. Lloret, K. Nakatani, H. Tokoro, S.-I. Ohkoshi, M. Verdaguer, Angew. Chem. Int. Ed. 51 (2012) 8356.
- [13] B. Das, D.C. Crans, J.B. Baruah, Inorg. Chim. Acta 408 (2013) 204.
- [14] K. Shankar, B. Das, J.B. Baruah, Eur. J. Inorg. Chem. (2013) 6147.
- [15] P. Pal, S. Konar, M.S.E. Fallah, K. Das, A. Bauzá, A. Frontera, S. Mukhopadhyay, RSC Adv. 5 (2015) 45082.
- [16] M. Mon, J. Vallejó, J. Pasán, O. Fabelo, C. Train, M. Verdaguer, S.-I. Ohkoshi, H. Tokoro, K. Nakagawa, E. Pardo, Dalton Trans. 46 (2017) 15130.
- [17] E. Pardo, C. Train, K. Boubekeur, G. Gontard, J. Cano, F. Lloret, K. Nakatani, M. Verdaguer, Inorg. Chem. 51 (2012) 11582.
- [18] T.U. Devi, A.J. Prabha, R. Meenakshi, G. Kalpana, C.S. Dilip, J. Phys. Sci. 28 (2017) 31.
- [19] U. Geiser, B.L. Ramakrishna, R.D. Willett, F.B. Hulsbergen, J. Reedijk, Inorg. Chem. 26 (1987) 3750.
   [20] D.R. Bloomquist, J.J. Jansen, C.P. Landee, R.D. Willet, R. Buder, Inorg. Chem. 20
- [20] D.R. Bloomquist, J.J. Jansen, C.P. Landee, R.D. Willet, R. Buder, Inorg. Chem. 20 (1981) 3308.
- [21] A.B. Caballero, O. Castillo, A. Rodríguez-Diéguez, J.M. Salas, Acta Crystallogr. E67 (2011) m1531.
- [22] J. Nenwa, E.D. Djomo, E.N. Nfor, P.L. Djonwouo, M. Mbarki, B.P.T. Fokwa, Polyhedron 99 (2015) 26.
- [23] M.A. Viswamitra, J. Chem. Phys. 37 (1962) 1408.
- [24] A. Earnshaw, Introduction to Magnetochemistry, Academic Press, London, 1968.
- [25] G.M. Sheldrick, SADABS, University of Göttingen, Göttingen, Germany, 2010.
- [26] G.M. Sheldrick, Acta Crystallogr. C71 (2015) 3.
- [27] K. Brandenburg, Diamond, Crystal Impact GbR, Bonn, Germany, 1999.
- [28] J. Nenwa, P.L. Djonwouo, E.N. Nfor, M.M. Bélombé, E. Jeanneau, M. Mbarki, B.P.T. Fokwa, Z. Naturforschung 69b (2014) 321.
- [29] D.T. Keene, M.B. Hursthouse, D.J. Price, Acta Crystallogr. E60 (2004) m378.
- [30] S. Alvarez, D. Avnir, M. Llunell, M. Pinsky, New J. Chem. 26 (2002) 996.
- [31] M.R. Sundberg, R. Kivekäs, J.K. Koskimies, J. Chem. Soc., Chem. Commun. (1991) 526.
- [32] R.S. Vilela, T.L. Oliveira, F.T. Martins, J.A. Ellena, F. Lloret, M. Julve, D. Cangussu, CR, Chimie 15 (2012) 856.
- [33] H.E. Ungnade, L.W. Kissinger, A. Narath, D.C. Barcham, J. Org. Chem. 28 (1963) 134
- [34] K. Nakamoto, Infrared Spectra of Inorganic Coordination Compounds, Wiley Ingerscience, New York, 1970.
- [35] S.L. Johnson, K.A. Rumon, J. Phys. Chem. 69 (1965) 74.
- [36] K. Muraleedharan, S. Kripa, J. Anal. Appl. Pyrolysis 107 (2014) 298.
- [37] K.V. Krishnamurty, G.M. Harris, Chem. Rev. 61 (1961) 213.
- [38] G. Gümüs, I. Gürol, F. Yuksel, A.G. Gürek, V. Ahsen, Polyhedron 33 (2012) 45.
- [39] S.K. Chattopadhyay, T.C.W. Mak, B.S. Luo, L.K. Thompson, A. Rana, S. Ghosh, Polyhedron 14 (1995) 3661.
- [40] A. Gleizes, F. Maury, J. Galy, Inorg. Chem. 19 (1980) 2074.
- [41] X. Zhou, Q. Chen, B. Liu, L. Li, T. Yang, W. Huang, Dalton Trans. 46 (2017) 430.
- [42] H. Oshio, U. Nagashima, Inorg. Chem. 31 (1992) 3295.
- [43] W. Li, H.P. Jia, Z.F. Ju, J. Zhang, Inorg. Chem. Commun. 11 (2008) 591.
- [44] O. Kahn, M.F. Charlot, Nouv. J. Chim. 4 (1980) 567.
- [45] I. Castro, J. Faus, M. Julve, M. Mollar, A. Monge, E. Gutiérrez-Puebla, Inorg. Chim. Acta 161 (1989) 97.
- [46] M.L. Calatayud, İ. Castro, J. Sletten, F. Lloret, M. Julve, Inorg. Chim. Acta 300 (2000) 846.
- [47] D. Cangussu, H.O. Stumpf, H. Adams, J.A. Thomas, F. Lloret, M. Julve, Inorg. Chim. Acta 358 (2005) 2292.
- [48] O. Castillo, A. Luque, P. Roman, F. Lloret, M. Julve, Inorg. Chem. 40 (2001) 5526.
- [49] O. Castillo, A. Luque, F. Lloret, P. Román, Inorg. Chim. Acta 324 (2001) 141.
- [50] M. Julve, A. Gleizes, L.M. Chamoreau, E. Ruiz, M. Verdaguer, Eur. J. Inorg. Chem. (2018) 509.
- [51] M.M. Bélombé, J. Nenwa, Y.A. Mbiangué, G. Bebga, F. Majoumo-Mbé, E. Hey-Hawkins, P. Lönnecke, Inorg. Chim. Acta 362 (2009) 1.
- [52] M.M. Bélombé, J. Nenwa, Y.A. Mbiangué, F. Majoumo-Mbé, P. Lönnecke, E. Hey- Hawkins, Dalton Trans. (2009) 4519.
- [53] G. Xu, K. Otsubo, T. Yamada, S. Sakaida, H. Kitagawa, J. Am. Chem. Soc. 135 (2013) 7438.
- [54] S.S. Nagarkar, S.M. Unni, A. Sharma, S. Kurungot, S.K. Ghosh, Angew. Chem. Int. Ed. 53 (2014) 2638.